


Mathematical modeling of microscale biology: Ion pairing, spatially varying permittivity, and Born energy in glycosaminoglycan brushes

William J. Ceely¹,* Marina Chugunova¹,† and Ali Nadim¹,‡

Institute of Mathematical Sciences, Claremont Graduate University, Claremont, California 91711, USA

James D. Sterling¹,§

Henry E. Riggs School of Applied Life Sciences, Keck Graduate Institute, Claremont, California 91711, USA

 (Received 29 June 2022; revised 3 October 2022; accepted 12 January 2023; published 23 February 2023)

Biological macromolecules including nucleic acids, proteins, and glycosaminoglycans are typically anionic and can span domains of up to hundreds of nanometers and even micron length scales. The structures exist in crowded environments that are dominated by multivalent electrostatic interactions that can be modeled using mean-field continuum approaches that represent underlying molecular nanoscale biophysics. We develop such models for glycosaminoglycan brushes using steady state modified Poisson-Boltzmann models that incorporate important ion-specific (Hofmeister) effects. The results quantify how electroneutrality is attained through ion electrophoresis, spatially-varying permittivity hydration forces, and ion-specific pairing. Brush-salt interfacial profiles of the electrostatic potential as well as bound and unbound ions are characterized for imposed jump conditions across the interface. The models should be applicable to many intrinsically-disordered biophysical environments and are anticipated to provide insight into the design and development of therapeutics and drug-delivery vehicles to improve human health.

DOI: [10.1103/PhysRevE.107.024416](https://doi.org/10.1103/PhysRevE.107.024416)

I. INTRODUCTION

Many biological structures are characterized by beds of intrinsically-disordered anionic biopolymers. In particular, nucleic acids, proteins, and extracellular glycosaminoglycans (GAGs) are polyelectrolytes that perform functions controlled by their hydration and their neutralization by cations and cationic residues of associated proteins. These anionic beds of slowly-diffusing macromolecules can be considered *fixed* in space over times scales of counterion neutralization phenomena. Although transient phenomena occur with molecular conformation changes, we can place the reference frame at the center of mass of the bed of the macromolecules to make analysis tractable. If the anionic bed is tethered to a tissue- or cell-surface, or a biopolymer is grafted to a surface, simplified structural models known as *brushes* can be defined and analysis can draw from a long history of brush research in polymer and surface science [1–4].

Another set of simplified structural models of anionic biopolymer beds are spherical *biomolecular condensates*. Here, nontethered anionic macromolecules interact with counterion atoms and molecules to form two coexisting liquid phases where a dense phase appears in the form of microscale spheres within a dilute phase. The discovery of biomolecular condensates (or *membraneless organelles*) has revolutionized

our perspective of biological structure and function, as the formation of condensates helps explain the acceleration of biochemical reaction rates and epigenetic control of biological processes that occur in both intracellular and extracellular domains [5,6]. In polymer science, such condensates fall within the broader category of *coacervates* as described in two recent review articles [7,8].

Pathologies associated with cell surfaces, mucosal surfaces, and membraneless organelles can be recapitulated in laboratory studies of biological structures that can be approximated as brushes and biocondensates. Thus, in a relatively new approach to drug discovery, biomacromolecules can be designed and applied to control microscale biology for therapeutic benefit. Examples include well-known polysaccharides such as heparin and hyaluronic acid as well as more recent cationic lipids used in mRNA vaccines [9], poly(acetyl, argyl) glucosamine (PAAG) for mucosal disorders [10], as well as cationic arginine-rich peptides for drug delivery applications [11].

In this paper, we develop a broadly-applicable mean-field mathematical model of anionic beds of macromolecules neutralized by cations focusing specifically on *GAG brushes* as a test case. The model aims to elucidate complexities of the biophysics of these molecularly-crowded environments where there is a delicate balance of multiple monovalent electrostatic ion pairing accompanied by release of water and ions upon binding. Calculations of the electrostatic coupling parameter (Table VI) from the data described in Sec. IV are less than unity suggesting weak coupling, but observed ion pairing indicates that modification of standard mean-field models is needed [12]. A steady state model is developed that depicts

*william.ceely@cgu.edu

†marina.chugunova@cgu.edu

‡ali.nadim@cgu.edu

§jim_sterling@kgi.edu

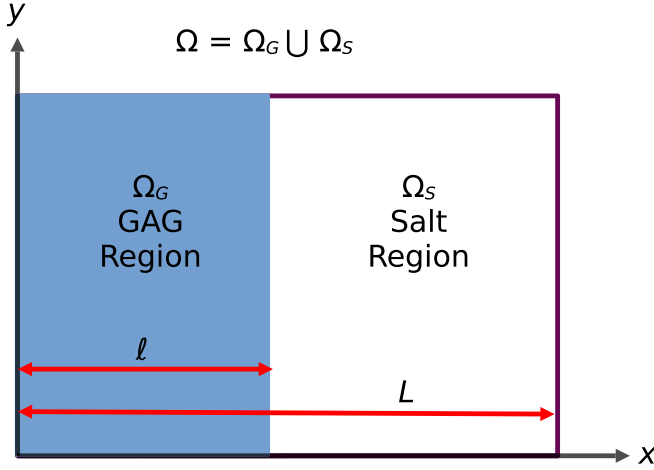


FIG. 1. Schematic of model depicting GAG brush region, $\Omega_G = \{0 \leq x \leq l\}$, salt region, $\Omega_S = \{l \leq x \leq L\}$, and total domain, $\Omega = \Omega_G \cup \Omega_S$.

steady state electrostatic interactions of a GAG brush in a bulk salt solution taking into account spatial variation of the permittivity, which leads to ion Born Hydration energy gradients, and ion pairing between the salt and the GAG brush. This model is known as a modified Poisson-Boltzmann (MPB) model.

We begin with the derivations of two MPB models using different assumptions for the variation of GAG brush-salt permittivity. We then compare our models to a previous model [13], which does not incorporate spatially-varying permittivity or ion pairing, showing how electrostatic potential and ion concentration profiles match in the limit and we compare results from both models. We then consider molecular simulation data [14], which show that varying permittivity and ion pairing lead to Born energy and a binding energy, respectively. We show how to relate the binding energy to our dissociation constant and compare predictions from our model to the simulation data. We then consider extensions to the models that include two counterions. Finally, we end with a discussion of our model applicability, its shortcomings, and future directions of this work.

II. THE STEADY-STATE MODEL

To derive a mathematical model to describe the electrostatics in Fig. 1, we begin, as normal, with the differential form of Gauss's law:

$$\nabla \cdot (\varepsilon \mathbf{E}) = \rho, \quad \text{in } \Omega, \quad (1)$$

where \mathbf{E} is the electric field, ρ is the total charge density, and ε is the permittivity of the medium. Assuming electrostatic conditions or that the magnetic field variation with time is negligible, the curl of the electric field can be assumed zero: $\nabla \times \mathbf{E} \approx \mathbf{0}$, so that we can define a relationship between the electric field and the potential as

$$\mathbf{E} = -\nabla\phi, \quad \text{in } \Omega. \quad (2)$$

Substituting (2) into (1), we arrive at

$$-\nabla \cdot (\varepsilon \nabla\phi) = \rho, \quad \text{in } \Omega. \quad (3)$$

The total charge density is related to the concentration of the unbound ions present:

$$\rho = \sum_i z_i N_A e [C_i], \quad (4)$$

where z_i is the valence and $[C_i]$ is the concentration of unbound ion i , respectively, N_A is Avogadro's constant, and e is the elementary charge. We make the simplifying assumption that the variation in potential and ion concentrations is only present in the x direction, which reduces our model to a single second order ordinary differential equation (ODE)

$$-\frac{d}{dx} \left(\varepsilon \frac{d\phi}{dx} \right) = \sum_i z_i N_A e [C_i], \quad \text{in } \Omega. \quad (5)$$

Finally, we focus on a negatively charged GAG in a monovalent salt solution and thus, $z_i = \pm 1$

$$-\frac{d}{dx} \left(\varepsilon \frac{d\phi}{dx} \right) = N_A e ([C^+] - [A^-] - [G^-]), \quad \text{in } \Omega, \quad (6)$$

where $[C^+]$ represents the cation concentration (such as Na^+ or K^+), $[A^-]$ represents the anion concentration (such as Cl^-), and $[G^-]$ represents the concentration of unbound negatively-charged groups attached to the fixed GAG molecules.

Previous models [13] assume a constant permittivity throughout the whole domain. However, molecular simulations [14] show a decrease in the permittivity within the GAG region. In what follows, we continue to develop our model using two different assumptions about how the permittivity and total concentration of the GAG vary throughout the domain. To this end, we incorporate a Born energy term [15] to account for this varying permittivity. The Born energy is given by

$$U_i = \frac{z_i^2 e^2}{8\pi \varepsilon r_i}, \quad (7)$$

where r_i is the Born radius of ion i . This is an effective radius and not a physically measured ion radius.

We also take into account ion pairing (the ability for the cation to bind to the GAG ions). In a reversible reaction, at equilibrium we must have $k_1 [G^-] [C^+] = k_{-1} [GC]$, which leads to

$$[GC] = \frac{[C^+]}{(k_{-1}/k_1)} [G^-] = \frac{[C^+]}{K_1} [G^-]. \quad (8)$$

Here $[GC]$ is the concentration of the GAG and the cation that are bound together, k_1 is the forward reaction rate constant at which the GAG and the cation bind together, k_{-1} is the backward reaction rate constant at which the bound GAG and cation break apart, and

$$K_1 \equiv \frac{k_{-1}}{k_1} \quad (9)$$

is known as the dissociation constant and has units of concentration.

The total GAG concentration, $[G^-]_0$, is the sum of the unbound GAG concentration, $[G^-]$, and the concentration of GAG that is bound to the cation, $[GC]$. Therefore, $[G^-]_0 = [G^-] + [GC] = [G^-](1 + [C^+]/K_1)$, resulting in

$$[G^-] = \frac{[G^-]_0}{(1 + [C^+]/K_1)}. \quad (10)$$

A. Piecewise constant permittivity and total GAG concentration

The simplest assumption that we can make for the varying permittivity and total GAG concentration is to assume piecewise constant values for both. This allows us to break the problem into two separate domains where the permittivity and the total GAG concentration are both constant.

Let

$$\varepsilon = \varepsilon_0 \varepsilon_r \varepsilon_x, \quad (11)$$

where ε_0 is the vacuum permittivity, ε_r is the dielectric constant of a reference medium, and

$$\varepsilon_x = \begin{cases} \varepsilon_S, & \text{in } \Omega_S \\ \varepsilon_G, & \text{in } \Omega_G \end{cases} \quad (12)$$

are constant scaling factors to the permittivity in the salt and GAG regions.

In the salt region, the total GAG concentration is taken to be zero. Thus, we can represent the ODE of Eq. (6) as

$$-\varepsilon_0 \varepsilon_r \varepsilon_S \frac{d^2 \phi}{dx^2} = N_A e ([C^+] - [A^-]), \quad \text{in } \Omega_S. \quad (13)$$

We scale all concentrations with some concentration, C_0 . Possible choices for C_0 are the bulk concentration of the salt or the total GAG concentration. Define the dimensionless concentrations as

$$c \equiv \frac{[C^+]}{C_0}, \quad a \equiv \frac{[A^-]}{C_0}. \quad (14)$$

Scale the electric potential, ϕ , with the thermal voltage

$$\frac{k_B T}{e} = \frac{N_A k_B T}{N_A e} = \frac{RT}{F}, \quad (15)$$

where k_B , T , R , and F are Boltzmann constant, absolute temperature, gas constant, and Faraday constant, respectively. Define the dimensionless potential as

$$y \equiv \frac{\phi}{(RT/F)}. \quad (16)$$

Substituting (14)–(16) into (13) and dividing both sides by F yields:

$$-\frac{\varepsilon_0 \varepsilon_r \varepsilon_S RT}{F^2 C_0} \frac{d^2 y}{dx^2} = c - a. \quad (17)$$

To nondimensionalize lengths, we define a modified Debye length, λ_D , as

$$\lambda_D^2 = \frac{\varepsilon_0 \varepsilon_r RT}{F^2 C_0}, \quad (18)$$

and scale x , ℓ , and L by λ_D . That is,

$$\hat{x} = \frac{x}{\lambda_D}, \quad \hat{\ell} = \frac{\ell}{\lambda_D}, \quad \hat{L} = \frac{L}{\lambda_D}. \quad (19)$$

Our dimensionless ODE in the salt region becomes

$$-\frac{d^2 y}{d\hat{x}^2} = \frac{1}{\varepsilon_S} (c - a), \quad \text{in } \Omega_S. \quad (20)$$

In crowded macromolecular environments, details of hydration can substantially impact ion motion and partitioning. Thus, assuming that the Born radii are the smallest length

scales [16], the ions partition according to Boltzmann distributions that combine electrostatic energy with Born hydration energy [17] (see Eq. (5.1) in [16]), and we can write:

$$c = \bar{c} \exp(-y - \hat{u}_c / \varepsilon_S), \quad (21)$$

$$a = \bar{a} \exp(y - \hat{u}_a / \varepsilon_S), \quad (22)$$

where $\hat{u}_c = e^2 / 8\pi k_B T \varepsilon_0 \varepsilon_r r_c$ and $\hat{u}_a = e^2 / 8\pi k_B T \varepsilon_0 \varepsilon_r r_a$ are the dimensionless Born energies in the reference medium with dielectric constant ε_r for the cation and anion, respectively. Estimating the length scales from molecular dynamic simulations of [14] indicate that the Born-augmented PB equation is appropriate. In the salt region this takes the explicit form:

$$-\frac{d^2 y}{d\hat{x}^2} = \frac{1}{\varepsilon_S} [\bar{c} \exp(-y - \hat{u}_c / \varepsilon_S) - \bar{a} \exp(y - \hat{u}_a / \varepsilon_S)], \quad \text{in } \Omega_S. \quad (23)$$

Since the potential is relative, we need to define the zero reference. We choose to define the reference potential where electroneutrality is locally met. That is, take $d^2 y / d\hat{x}^2 \equiv 0$, where $y = 0$ in Ω_S , so that

$$0 = \bar{c} \exp(-\hat{u}_c / \varepsilon_S) - \bar{a} \exp(-\hat{u}_a / \varepsilon_S). \quad (24)$$

This can be written as $\tilde{c} = \tilde{a}$, where $\tilde{c} = \bar{c} \exp(-\hat{u}_c / \varepsilon_S)$ and $\tilde{a} = \bar{a} \exp(-\hat{u}_a / \varepsilon_S)$ are rescaled dimensionless concentrations in the bulk salt solution.

The final version of the governing equations, known as the Born-energy augmented Poisson-Boltzmann equation [16], reduce to the following. In the salt region we have

$$-\frac{d^2 y}{d\hat{x}^2} = \frac{\tilde{c}}{\varepsilon_S} [e^{-y} - e^y], \quad \text{in } \Omega_S. \quad (25)$$

In the GAG region, the total GAG concentration, $[G^-]_0$, is taken to be constant, whereby

$$-\varepsilon_0 \varepsilon_r \varepsilon_G \frac{d^2 \phi}{dx^2} = N_A e \left([C^+] - [A^-] - \frac{[G^-]_0}{(1 + [C^+]/K_1)} \right), \quad \text{in } \Omega_G. \quad (26)$$

Using the same scaling parameters (C_0 , RT/F , λ_D) from the salt region derivation we obtain:

$$-\frac{d^2 y}{d\hat{x}^2} = \frac{1}{\varepsilon_G} \left[c - a - \frac{\bar{g}}{1 + c/\tilde{K}_1} \right], \quad \text{in } \Omega_G, \quad (27)$$

where $\bar{g} = [G^-]_0 / C_0$ and $\tilde{K}_1 = K_1 / C_0$. Again, assuming Boltzmann distributions combined with Born energy for the mobile ions:

$$c = \tilde{c} \exp \left(-y - \hat{u}_c \left[\frac{1}{\varepsilon_G} - \frac{1}{\varepsilon_S} \right] \right), \quad (28)$$

$$a = \tilde{c} \exp \left(y - \hat{u}_a \left[\frac{1}{\varepsilon_G} - \frac{1}{\varepsilon_S} \right] \right). \quad (29)$$

Substitute Eqs. (28) and (29) into (27) to arrive at the final version of the ODE in the GAG region. The value of the dimensionless potential, y , that makes the right-hand side zero is known as the Donnan potential, y_D .

Thus, the model assuming piecewise constant permittivity and total GAG concentration is complete with Eqs. (25) and (27)–(29) along with the boundary conditions:

$$y(\hat{\ell}^-) = y(\hat{\ell}^+), \quad (30a)$$

$$\varepsilon_G \frac{d}{d\hat{x}} y(\hat{\ell}^-) = \varepsilon_S \frac{d}{d\hat{x}} y(\hat{\ell}^+), \quad (30b)$$

$$-\frac{d}{d\hat{x}} y(0) = \hat{\sigma}_2, \quad (30c)$$

$$\frac{d}{d\hat{x}} y(\hat{L}) = \hat{\sigma}_1. \quad (30d)$$

The first two conditions equate the potential and positive and negative surface charge densities at the interface. For electroneutrality to hold overall, we must have $\hat{\sigma}_1 = -\hat{\sigma}_2$. These are the surface charge densities at the two boundaries.

B. Smoothly varying permittivity and total GAG concentration

Perhaps a more accurate assumption for the varying permittivity and total GAG concentration is to take them to vary smoothly with respect to x rather than being discontinuous at the interface. The same MPB equation thus holds throughout the domain:

$$-\varepsilon_0 \varepsilon_r \frac{d}{dx} \left(\varepsilon_1(x) \frac{d\phi}{dx} \right) = N_A e ([C^+] - [A^-] - [G^-]). \quad (31)$$

Using the same scaling parameters (C_0 , RT/F , λ_D , \hat{u}_c , and \hat{u}_a) from Sec. II A, the dimensionless ODE becomes

$$-\varepsilon_1(\hat{x}) \frac{d^2 y}{d\hat{x}^2} - \frac{d\varepsilon_1(\hat{x})}{d\hat{x}} \frac{dy}{d\hat{x}} = c - a - \frac{\bar{g}(\hat{x})}{1 + c/K_1}, \quad \text{in } \Omega, \quad (32)$$

where

$$c = \bar{c} \exp \left(-y - \frac{\hat{u}_c}{\varepsilon_1(\hat{x})} \right), \quad (33)$$

$$a = \bar{a} \exp \left(y - \frac{\hat{u}_a}{\varepsilon_1(\hat{x})} \right), \quad (34)$$

with boundary conditions

$$-\frac{d}{d\hat{x}} y(0) = \hat{\sigma}_2, \quad (35a)$$

$$\frac{d}{d\hat{x}} y(\hat{L}) = \hat{\sigma}_1. \quad (35b)$$

To complete the model, we need to define the smooth functions $\varepsilon_1(\hat{x})$ and $\bar{g}(\hat{x})$. A convenient choice for a smooth function is the hyperbolic tangent. Let

$$f(\hat{x}) = \frac{1}{2} \left[\tanh \left(\frac{1 - \hat{x}/\hat{\ell}}{\alpha} \right) + 1 \right]. \quad (36)$$

The transition is centered at $\hat{x} = \hat{\ell}$, and $\alpha > 0$ controls the transition length. We then define

$$\bar{g}(\hat{x}) \equiv g_0 f(\hat{x}), \quad (37)$$

$$\varepsilon_1(\hat{x}) \equiv (\varepsilon_G - \varepsilon_S) f(\hat{x}) + \varepsilon_S. \quad (38)$$

We can express \bar{a} in terms of \bar{c} by defining the first and second derivative of y to be zero when $y = 0$, noting that $\varepsilon_1 \approx \varepsilon_S$ and $\bar{g} \approx 0$ in this case. With this we see that

$$\bar{a} = \bar{c} \exp \left(\frac{\hat{u}_a - \hat{u}_c}{\varepsilon_S} \right). \quad (39)$$

We argue that this model is equivalent to the model (25) and (27)–(30) in the limit. With the proposed smooth function, for $\alpha \ll 1$, the permittivity and total GAG concentration are essentially piecewise constant except for near the interface ($\hat{x} \approx \hat{\ell}$). So the model (25) and (27)–(30) is an approximation to this model away from the interface. Further, we also note that as $\alpha \rightarrow 0$,

$$f(\hat{x}) \rightarrow \begin{cases} 1, & \text{in } \Omega_G \\ 0, & \text{in } \Omega_S \end{cases}, \quad (40)$$

that is, $f(\hat{x})$ approaches a piecewise constant function, and this version of the model approaches that of (25) and (27)–(30).

Figures 3–7 show solutions of this model with the input parameters described in Table IV. These results are discussed in Sec. IV C.

III. PREVIOUS VOLUME CHARGE MODEL: GAG BRUSH NEAR A CHARGED SURFACE

A. Brief description of the model

Dean *et al.* [13] provide three mathematical PB models to describe the electrostatic interactions of a negatively charged chondroitin sulfate GAG in a bulk NaCl salt solution. The basic form of the models is

$$\nabla^2 \Phi = \frac{2FC_0}{\varepsilon_w} \sinh \left(\frac{F\Phi}{RT} \right) - \frac{\rho_{\text{fix}}}{\varepsilon_w}, \quad (41)$$

where C_0 is the bath concentration of NaCl, ρ_{fix} is a fixed charge density term, and ε_w is the permittivity of the bulk solution.

The volume charge model in Fig. 2 approximates the GAG brush as a fixed uniform volume charge density of height, h . Inside the GAG brush region, the ODE has the form

$$\nabla^2 \Phi = \frac{2FC_0}{\varepsilon_w} \sinh \left(\frac{F\Phi}{RT} \right) - \frac{\rho_{\text{volume}}}{\varepsilon_w}, \quad (42)$$

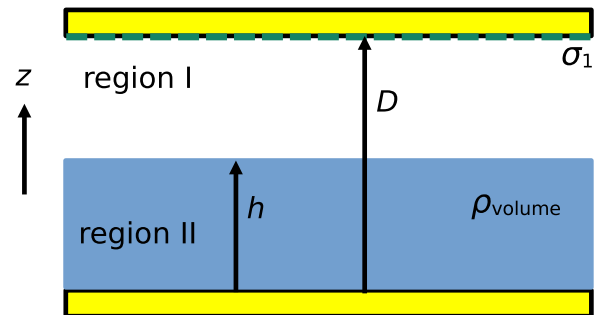


FIG. 2. Schematic of constant volume charge model depicting GAG brush with constant volume charge density, ρ_{volume} , in region II of height, h , bulk salt in region I extending from $h \leq z \leq D$, and surface charge density, σ_1 . Recreated from [13].

TABLE I. Parameters from [13].

Parameters	Volume model
σ_1 (C/m ²)	-0.015
σ_2 (C/m ²)	0
Q (C)	-8.00×10^{-18}
s (nm)	6.5
h (nm)	20
D (nm)	30
ρ_{volume} (C/m ³)	$Q/(s^2h)$
T (K)	298
ε_w (C ² /N m ²)	6.92×10^{-10}
C_0 (M)	0.01, 0.1, 1.0

and in the salt region, the ODE has the form

$$\nabla^2 \Phi = \frac{2FC_0}{\varepsilon_w} \sinh\left(\frac{F\Phi}{RT}\right). \quad (43)$$

The boundary conditions are given as

$$\frac{\partial}{\partial z} \Phi(0) = 0, \quad (44a)$$

$$\frac{\partial}{\partial z} \Phi(D) = \frac{\sigma_1}{\varepsilon_w}, \quad (44b)$$

$$\Phi(h^-) = \Phi(h^+), \quad (44c)$$

$$\frac{\partial}{\partial z} \Phi(h^-) = \frac{\partial}{\partial z} \Phi(h^+). \quad (44d)$$

B. Relationship between models

The models in [13] assume a constant permittivity throughout both the salt and GAG regions. In our model, this would imply $\varepsilon_S = \varepsilon_G = 1$ and thus, $\varepsilon_w = \varepsilon_0 \varepsilon_r$. Nondimensionalizing the ODEs, using the same scaling parameters from our model, and replacing z with x :

$$\frac{d^2y}{d\hat{x}^2} = 2\bar{c} \sinh(y) = \bar{c}[e^y - e^{-y}], \quad \text{in I,} \quad (45)$$

$$\frac{d^2y}{d\hat{x}^2} = \bar{c}[e^{-y} - e^y] - \frac{\rho_{\text{volume}}}{FC_0}, \quad \text{in II.} \quad (46)$$

These are similar to our model in Eqs. (25) and (27), with two important differences. The first is that [13] does not include a Born energy term. However, because the permittivity is assumed constant, the Born energy would also be constant. Therefore, it could be lumped into the dimensionless concentration \bar{c} , which matches our \tilde{c} . The second difference is that [13] ignores any ion pairing. In other words, the total GAG concentration is equal to the unbound GAG concentration. If we allow the dissociation constant to approach ∞ , then $[G^-] \rightarrow -\rho_{\text{volume}}$, and we see that our model approaches the model in [13] in the limit.

Table I summarizes the parameters used in [13]. Table II summarizes the input parameters needed for our model (25) and (27)–(30) and how they relate to the values in Table I. Note that since the permittivity is constant, the terms $\hat{u}_c[1/\varepsilon_G - 1/\varepsilon_S]$ and $\hat{u}_a[1/\varepsilon_G - 1/\varepsilon_S]$ from equations (28) and (29) are zero and not needed. Using the model equations from [13] [summarized in equations (43)–(44d)], with the parameters summarized in Table I, we replicated the predicted profiles for potential, ϕ , and both the cation and anion concentration. We then used our model (25) and (27)–(30), with the parameters summarized in Table II to generate the same profiles. The results are in perfect agreement, further showing that in the limit, our model approaches the volume charge model in [13].

IV. PREVIOUS MOLECULAR DYNAMICS SIMULATIONS: GAG BRUSH-SALT INTERFACE

A. Brief description of molecular simulations

Sterling *et al.* [14] performed all-atom molecular dynamics nanoscale simulations of hyaluronic acid (HA) and oversulfated heparin (HS) GAG brushes in NaCl and KCl solutions. The results of the simulation are reported for the average brush values, represented by subscript b relative to values in the bulk salt layer denoted by subscript o including the Donnan potential, variation of the permittivity, Born energy

TABLE II. Input parameters to piecewise constant permittivity and total GAG concentration model.

Parameter	Notes	Value for $C_0 = 0.01$	Value for $C_0 = 0.1$	Value for $C_0 = 1$
ε_r	$\varepsilon_0/\varepsilon_w$	78.155	78.155	78.155
ε_S	Constant ε_w	1	1	1
ε_G	Constant ε_w	1	1	1
$\hat{\ell}$	h/λ_D	4.660	14.737	46.603
\hat{L}	D/λ_D	6.990	22.106	69.904
\tilde{K}_1	No binding	10^{16}	10^{16}	10^{16}
\tilde{c}	C_0/C_0	1	1	1
\bar{g}	$-\frac{\rho_{\text{volume}}}{FC_0}$	9.812	9.812×10^{-1}	9.812×10^{-2}
$\hat{\sigma}_1$	$\frac{\sigma_1 F \lambda_D}{\varepsilon_w RT}$	-3.623	-1.146	-0.362
$\hat{\sigma}_2$	$\frac{-\sigma_2 F \lambda_D}{\varepsilon_w RT}$	0	0	0

and the total concentrations of the ions. Thus, a Born-modified Boltzmann partitioning with ion-pair binding is proposed as

$$c_{i,b} = c_{i,o} \exp \left(-\frac{q_i \varphi_b}{k_B T} - \frac{-\Delta G_i^s}{k_B T} \frac{\varepsilon_w}{\varepsilon_w - 1} \left[\frac{1}{\varepsilon_b} - \frac{1}{\varepsilon_o} \right] - \frac{\Delta \mu_i}{k_B T} \right), \quad (47)$$

where the first term represents the ion charge q_i in Donnan potential φ_b , the second term is the Born energy term, the third term represents the ion-pair binding free energy between ion atoms and brush anionic charges.

B. Relationship between simulation data and model

In [14], the simulation models consisted of a bulk solution occupying $z = -240 \text{ \AA}$ to 240 \AA and GAG brushes of varying lengths, 2ℓ , centered at $z = 0$. Our model only considers the positive half of this domain $x = 0$ to 240 \AA with the GAG brush occupying $x = 0$ to $\ell \text{ \AA}$. With zero-gradient boundary conditions at 0 and ℓ , we model the interface between an infinite brush and infinite salt layer. The conditions relating quantities far from the interface represent so-called *jump conditions* that are analogous to the Rankine-Hugoniot conditions that are imposed across shock wave interfaces.

In the results from [14], total concentrations are used instead of those of the unbound charged ions, and a cation binding energy term is introduced. Rewriting Eqs. (27)–(29) to incorporate the binding energy and use total concentrations (instead of unbound concentrations):

$$-\frac{d^2 y}{d\hat{x}^2} = \frac{\tilde{c}}{\varepsilon_G} \left\{ \exp \left(-y - \hat{u}_c \left[\frac{1}{\varepsilon_G} - \frac{1}{\varepsilon_S} \right] - \frac{\Delta \mu}{k_B T} \right) - \exp \left(y - \hat{u}_a \left[\frac{1}{\varepsilon_G} - \frac{1}{\varepsilon_S} \right] \right) \right\} - \frac{\bar{g}}{\varepsilon_G}. \quad (48)$$

When $y = y_D$,

$$\bar{g} = \tilde{c} \left\{ \exp \left(-y_D - \hat{u}_c \left[\frac{1}{\varepsilon_G} - \frac{1}{\varepsilon_S} \right] - \frac{\Delta \mu}{k_B T} \right) - \exp \left(y_D - \hat{u}_a \left[\frac{1}{\varepsilon_G} - \frac{1}{\varepsilon_S} \right] \right) \right\}. \quad (49)$$

To find a relationship between the binding energy and the dissociation constant, substitute this into (27) with $y = y_D$ and solve for \tilde{K}_1 :

$$\tilde{K}_1 = \frac{\tilde{c} \{ e^{(-y_D - \hat{u}_c [\frac{1}{\varepsilon_G} - \frac{1}{\varepsilon_S}])} - e^{(y_D - \hat{u}_a [\frac{1}{\varepsilon_G} - \frac{1}{\varepsilon_S}])} \}}{e^{(-\frac{\Delta \mu}{k_B T})} - 1}. \quad (50)$$

The above relationships are only valid at the Donnan potential, to compute the binding energy for any potential, set

the right-hand sides of (27) and (48) equal and solve for $\exp(-\Delta \mu/(k_B T))$:

$$\exp \left(-\frac{\Delta \mu}{k_B T} \right) = 1 + \frac{\bar{g}}{\tilde{K}_1 + \tilde{c} \exp \left(-y - \hat{u}_c \left[\frac{1}{\varepsilon_G} - \frac{1}{\varepsilon_S} \right] \right)}. \quad (51)$$

Similarly, using Eq. (32) instead of (27), and noting that $\varepsilon_1(\hat{x}) = \varepsilon_G$ deep in the brush where the Donnan potential occurs, we find the relationships to be

$$\tilde{K}_1 = \frac{\bar{c} \exp \left(-y_D - \frac{\hat{u}_c}{\varepsilon_G} \right) - \bar{a} \exp \left(y_D - \frac{\hat{u}_a}{\varepsilon_G} \right)}{\exp \left(-\frac{\Delta \mu}{k_B T} \right) - 1}, \quad (52)$$

or

$$\exp \left(-\frac{\Delta \mu}{k_B T} \right) = 1 + \frac{\bar{g}}{\tilde{K}_1 + \bar{c} \exp \left(-y - \frac{\hat{u}_c}{\varepsilon_1(\hat{x})} \right)}. \quad (53)$$

This can be used to compute the total cation concentration in addition to the unbound concentration.

C. Summary and comparison of results

Table III summarizes the parameters needed from [14] to generate the input parameters to the model (32)–(35). The input parameters are listed in Table IV. Based on the literature, we expected the Born radius for chloride to be 2.26 \AA [18]. However, by using this value in our model, we found that chloride would not be excluded from the brush as in the molecular simulation results. This led to a negative concentration of unbound GAG ions, a negative dissociation constant, and/or the inability to match the Donnan potential. By reducing the Born radius for chloride by a factor of ten, our model was able to overcome these issues. Table IV shows the values of \hat{u}_a , \tilde{K}_1 , and \bar{a} based on the actual value of 0.226 \AA used in our model.

The value of α to control the transition length of the permittivity and total GAG concentration functions was qualitatively varied until the results in Table V and the total charge density curves in Fig. 6(c) were in agreement with the corresponding data in [14].

As seen in Table V, our model predictions are well within the standard deviations from the molecular simulation results. All of our predicted energy values are within 0.014 of the average values obtained from the molecular simulations.

The electrostatic coupling parameter, Ξ , can be calculated by $\Xi = 2\pi z^3 \lambda_B^2 |\sigma|$ [12]. The valency of the cation is z , which is equal to one for all four scenarios we used, $\lambda_B = e^2/(4\pi \varepsilon_r \varepsilon_0 k_B T)$ is the Bjerrum length, and $-\sigma e$ is the effective net surface charge density at the interface between the GAG and salt regions. This surface charge density is computed by integrating the net volumetric charge density across the entire GAG region which is approximately 60 \AA

TABLE III. Parameters from [14].

GAG	Salt	Bulk salt conc. (M)	GAG conc. (M)	Polymer length (\AA)	ε_b	ε_o	T (K)
Hyaluronan	NaCl	0.28	0.51	129.7	50.7	60.4	310.15
	KCl	0.28	0.49	135.8	51.2	61.8	310.15
Heparin	NaCl	0.27	2.78	119.3	37.5	59.1	310.15
	KCl	0.26	2.93	113.2	37.9	60.5	310.15

TABLE IV. Input parameters to smoothly varying permittivity and total GAG concentration model.

Parameter	Notes	Hyaluronan NaCl	Hyaluronan KCl	Heparin NaCl	Heparin KCl
ϵ_r	Dilute water, ϵ_w	78.155	78.155	78.155	78.155
$\epsilon_1(\hat{L}) = \epsilon_S$	ϵ_o/ϵ_r	0.773	0.791	0.756	0.774
$\epsilon_1(0) = \epsilon_G$	ϵ_b/ϵ_r	0.649	0.655	0.480	0.485
$\hat{\ell}$	Polymer length/ $2/\lambda_D$	7.838	8.206	7.079	6.592
\hat{L}	240 Å/ λ_D	29.007	29.007	28.484	27.951
r_c (Å)	[18]	1.62	1.95	1.62	1.95
\hat{u}_c	Based on r_c	2.128	1.768	2.128	1.768
r_a (Å)	Sec. IV C	0.226	0.226	0.226	0.226
\hat{u}_a	Based on used r_a	15.251	15.251	15.251	15.251
C_0	Salt concentration	0.28	0.28	0.27	0.26
\tilde{K}_1	Eq. (52)	0.172	0.114	1.337×10^{-2}	8.735×10^{-4}
\tilde{c}	Salt concentration/ C_0	1	1	1	1
\tilde{c}	$\tilde{c} \exp(\hat{u}_c/\epsilon_S)$	15.692	9.350	16.671	9.810
\tilde{a}	$\tilde{c} \exp[(\hat{u}_a - \hat{u}_c)/\epsilon_S]$	3.721×10^8	2.380×10^8	5.744×10^8	3.602×10^8
g_0	GAG concentration/ C_0	1.821	1.75	10.297	11.269
$\hat{\sigma}_1$		0	0	0	0
$\hat{\sigma}_2$		0	0	0	0
α	Used value	0.1	0.1	0.1	0.1

wide. Table VI shows the calculated values of λ_B , σ , and Ξ based on the molecular simulation and our model results. For all four scenarios $\Xi < 1$, indicating that for our systems of interest, we are in the weak coupling regime, thus justifying the mean-field approach.

Plots of the predicted dimensionless potential, unbound charge density and total charge density curves can be found in Figs. 3–6. For Figs. 4 and 6, representing brushes with a potassium cation, the net charge density curves exhibit a double-double layer of negative charge just outside of the brush edge and positive charge just inside of the brush edge. Observing the electrostatic potential, we see the same trend as expected in a dilute-limit where varying permittivity effects are negligible: a negative unbound charge density at an x location corresponds to a positive second derivative in the electrostatic potential, while a positive unbound charge density corresponds to a negative second derivative in the electrostatic potential. The molecular simulation data in [14] exhibited the opposite trend, positive charge just outside of the brush, and negative charge just inside of the brush. This is the only substantial difference between our model predictions and the molecular simulation data.

In contrast to the GAG brush results for the potassium cation, the net charge density curves in Figs. 3 and 5 in the presence of a sodium cation show more complex structure. The brushes exhibit a negative charge inside the edge of the brush, then a positive charge in the transition region, and a negative charge on the outside edge of the brush. This corresponds to an electrostatic potential second-derivative that is positive-negative-positive, meaning there is a substantial *overshoot* of the potential rather than a smooth transition in the potential curve.

Combining the Coulomb force, $F = qE$, with Eqs. (2) and (4), we can define a dimensionless net Coulomb force density

$$f = -(c - a - g) \frac{dy}{dx}. \tag{54}$$

From Fig. 7, we see that the net force density is zero everywhere except in a region near the boundary between the GAG and salt regions. We see that for Heparin KCl [Fig 7(b)] there is a *pinching* effect at the boundary where the force in the GAG region at the boundary is toward the right (salt region) and the force in the salt region at the boundary is toward the left (GAG region). Such a force calculation is more

TABLE V. Dimensionless energy results molecular simulation vs model prediction.

GAG	Salt		Donnan potential	Born hydration energy	Cation binding energy
Hyaluronan	NaCl	Molecular simulation [14]	0.17 ± 0.06	0.53 ± 0.2	-1.32 ± 0.2
		Model prediction	0.175	0.527	-1.316
Hyaluronan	KCl	Molecular simulation [14]	0.44 ± 0.03	0.46 ± 0.2	-1.46 ± 0.2
		Model prediction	0.430	0.463	-1.469
Heparin	NaCl	Molecular simulation [14]	-0.62 ± 0.27	1.62 ± 0.6	-3.35 ± 0.6
		Model prediction	-0.611	1.621	-3.342
Heparin	KCl	Molecular simulation [14]	0.96 ± 0.14	1.36 ± 0.5	-4.73 ± 0.5
		Model prediction	0.946	1.362	-4.730

TABLE VI. Electrostatic coupling parameter.

Parameter	Hyaluronan NaCl	Hyaluronan KCl	Heparin NaCl	Heparin KCl
Bjerrum length, λ_B (Å)	6.894	6.894	6.894	6.894
Equivalent net surface charge density, σ (m^{-2})	1.693×10^{16}	2.437×10^{16}	1.548×10^{16}	4.223×10^{16}
Electrostatic coupling parameter, Ξ (dimensionless)	0.051	0.073	0.046	0.126

complicated when there is an overshoot in potential as seen in Figs. 3 and 5 for GAG brushes with a sodium cation. In these cases, the Coulombic force traversing the brush edge is right-left-right-left [Fig 7(a)] and Born hydration forces along with polymer elastic forces also need to be considered in the force balance.

V. TWO CATION PARTITIONING

The model as derived above focused on a monovalent salt solution consisting of one cation and one anion. This can be expanded to incorporate a second cation by modifying Eq. (6) to be

$$-\frac{d}{dx} \left(\varepsilon \frac{d\phi}{dx} \right) = N_A e ([C_1^+] + [C_2^+] - [A^-] - [G^-]), \quad \text{in } \Omega, \quad (55)$$

where $[C_1^+]$ represents the cation one concentration and $[C_2^+]$ represents the cation two concentration. There are now two ion pairs, which leads to the modified equation (8) as

$$[GC_1] = \frac{[C_1^+]}{K_1} [G^-], \quad [GC_2] = \frac{[C_2^+]}{K_2} [G^-], \quad (56)$$

where K_1 and K_2 are the dissociation constants for cations one and two, respectively.

The total GAG concentration, $[G^-]_0$, is now the sum of the unbound GAG concentration, $[G^-]$, and the concentrations of the two bound ion pairs, $[GC_1]$ and $[GC_2]$, i.e., $[G^-]_0 =$

$[G^-] + [GC_1] + [GC_2]$. From this, we infer that

$$[G^-] = \frac{[G^-]_0}{1 + [C_1^+]/K_1 + [C_2^+]/K_2}. \quad (57)$$

For more than two cations, this generalizes to $[G^-] = \frac{[G^-]_0}{1 + \sum_i [C_i^+]/K_i}$. If desired, pH can be incorporated into this formulation by considering hydronium as one type of cation.

A. Smooth model

Following the same procedure and definitions from Sec. II B, we arrive at the modified smooth model ODE

$$-\varepsilon_1(\hat{x}) \frac{d^2 y}{d\hat{x}^2} - \frac{d\varepsilon_1(\hat{x})}{d\hat{x}} \frac{dy}{d\hat{x}} = c_1 + c_2 - a - \frac{\bar{g}(\hat{x})}{1 + \frac{c_1}{K_1} + \frac{c_2}{K_2}}, \quad \text{in } \Omega, \quad (58)$$

where

$$c_1 = \bar{c}_1 \exp\left(-y - \frac{\hat{u}_{c1}}{\varepsilon_1(\hat{x})}\right), \quad (59)$$

$$c_2 = \bar{c}_2 \exp\left(-y - \frac{\hat{u}_{c2}}{\varepsilon_1(\hat{x})}\right), \quad (60)$$

$$a = \bar{a} \exp\left(y - \frac{\hat{u}_a}{\varepsilon_1(\hat{x})}\right), \quad (61)$$

$$\bar{a} = \bar{c}_1 \exp\left(\frac{\hat{u}_a - \hat{u}_{c1}}{\varepsilon_S}\right) + \bar{c}_2 \exp\left(\frac{\hat{u}_a - \hat{u}_{c2}}{\varepsilon_S}\right). \quad (62)$$

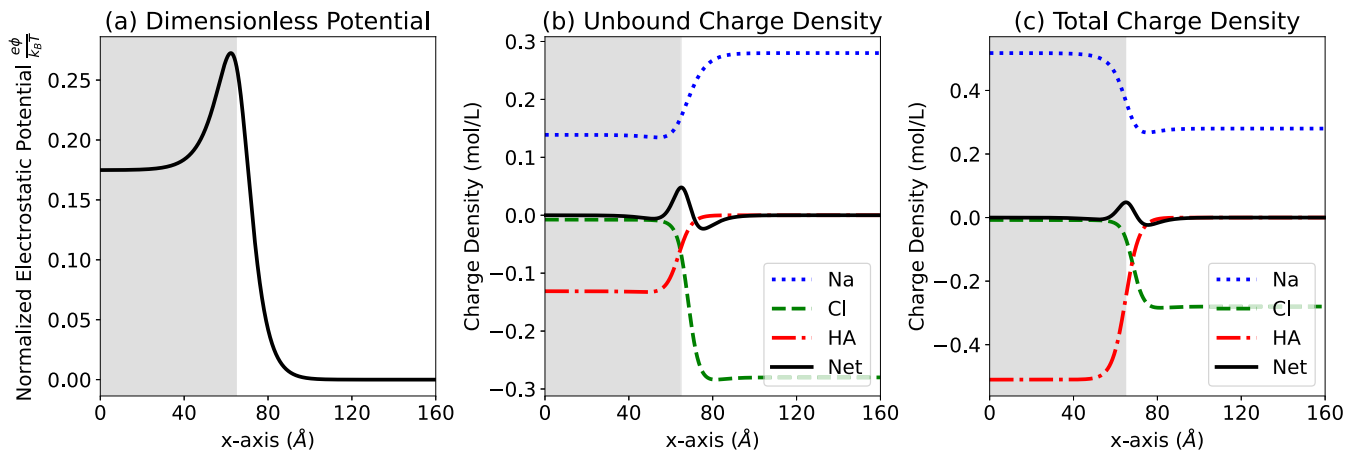


FIG. 3. Hyaluronan NaCl results. (a) Dimensionless potential, (b) unbound charge density (M), and (c) total charge density (M) using parameters from Table IV. In (b) and (c), the dotted blue curve represents Na, the dashed green curve represents Cl, the dashed dot red curve represents Hyaluronan, and the solid black curve represents the net charge density. All curves continue flat from 160 to 240 Å. Shaded region represents the GAG region.

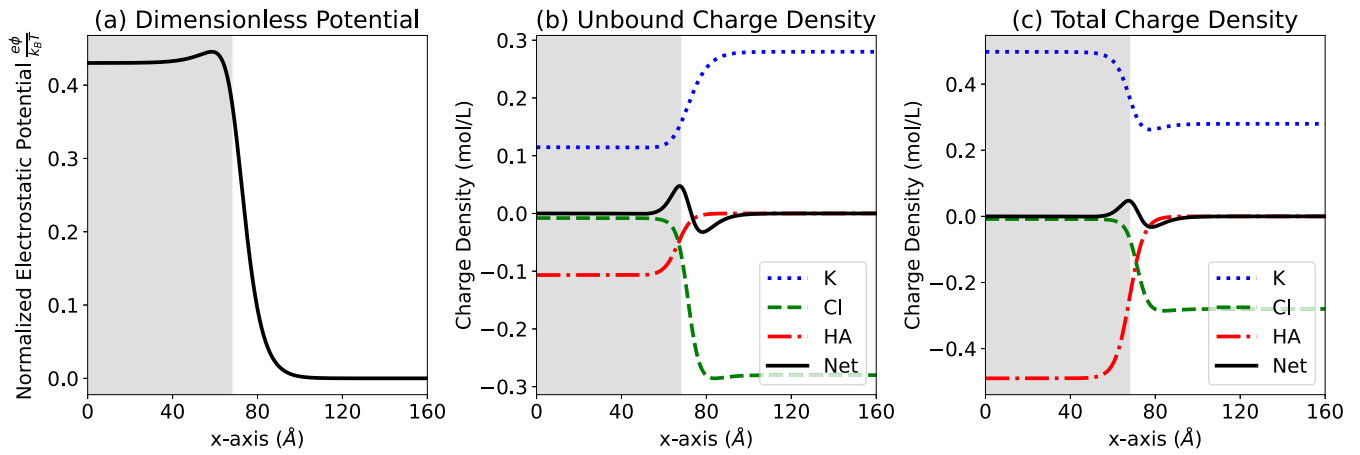


FIG. 4. Hyaluronan KCl results. (a) Dimensionless potential, (b) unbound charge density (M), and (c) total charge density (M) using parameters from Table IV. In (b) and (c), the dotted blue curve represents K, the dashed green curve represents Cl, the dashed dot red curve represents Hyaluronan, and the solid black curve represents the net charge density. All curves continue flat from 160 to 240 Å. Shaded region represents the GAG region.

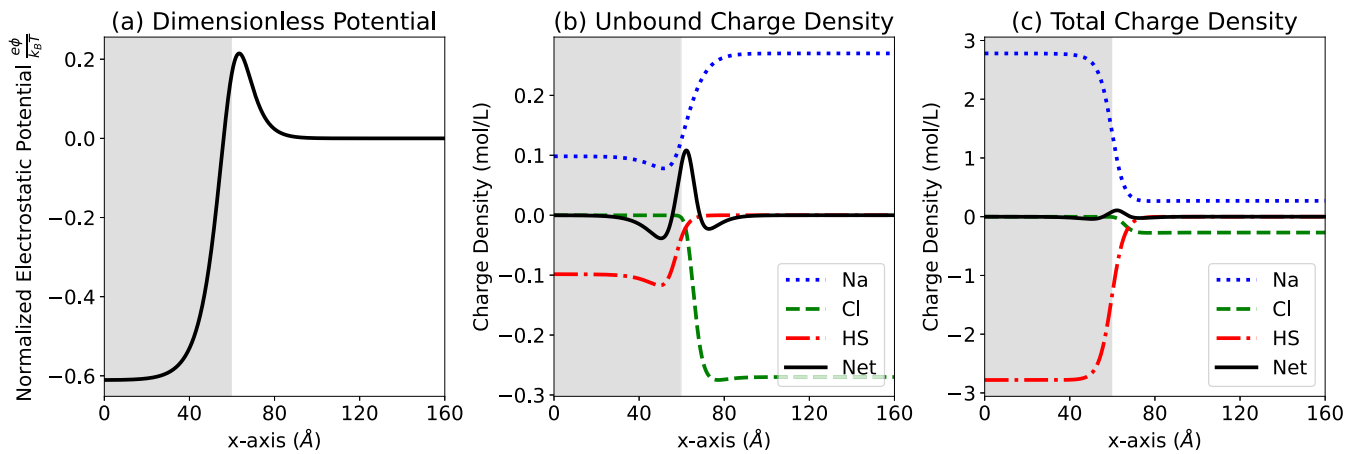


FIG. 5. Heparin NaCl results. (a) Dimensionless potential, (b) unbound charge density (M), and (c) total charge density (M) using parameters from Table IV. In (b) and (c), the dotted blue curve represents Na, the dashed green curve represents Cl, the dashed dot red curve represents Heparin, and the solid black curve represents the net charge density. All curves continue flat from 160 to 240 Å. Shaded region represents the GAG region.

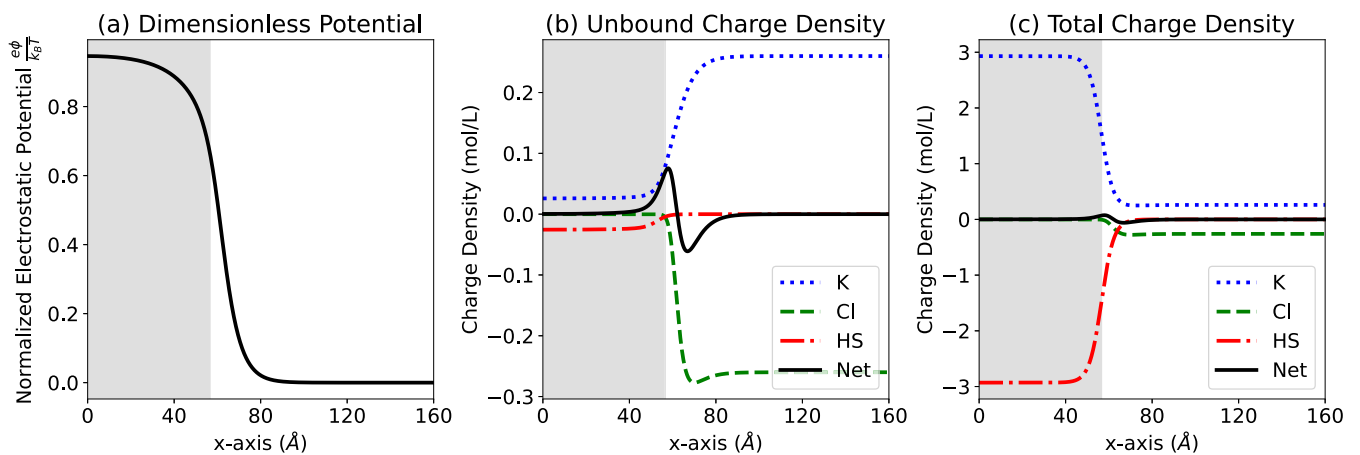


FIG. 6. Heparin KCl results. (a) Dimensionless potential, (b) unbound charge density (M), and (c) total charge density (M) using parameters from Table IV. In (b) and (c), the dashed blue curve represents K, the dotted green curve represents Cl, the dashed dot red curve represents Heparin, and the solid black curve represents the net charge density. All curves continue flat from 160 to 240 Å. Shaded region represents the GAG region.

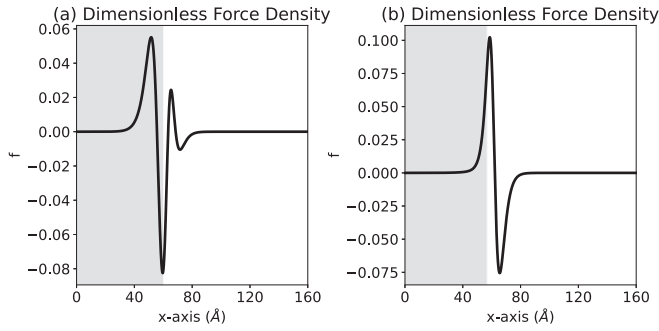


FIG. 7. Dimensionless force density for (a) Heparin NaCl and (b) Heparin KCl.

The boundary conditions remain unchanged from Eqs. (35a)–(35b).

The piecewise constant model can be obtained as before by letting $\alpha \rightarrow 0$.

B. Sample result for sodium and potassium

To produce some sample results for the extended model with two cations, input parameters were generated by averaging the parameters from Tables III and IV for the Heparin NaCl and Heparin KCl scenarios. However, the salt side concentrations were chosen such that the total number of sodium ions and potassium ions in the whole domain are equal in order to demonstrate how they differentially partition into the brush based on their respective Born radii and dissociation constants. The values used are captured in Table VII where c_1 represents sodium and c_2 represents potassium.

The sample results are captured in Figs. 8 and 9. For the given input parameters, it is seen that in the brush side, there is almost no unbound potassium. Essentially all of the potassium ions in the brush side are bound with the GAG brush. Sodium, on the other hand, exists in the brush as both bound and unbound ions, but the total sodium concentration is just more than half of the total potassium concentration. This

TABLE VII. Input parameters for sample two cation scenario.

Parameter	Notes	Value
ε_r	Dilute water, ε_w	78.155
$\varepsilon_1(\hat{L}) = \varepsilon_S$	$\varepsilon_o/\varepsilon_r$	0.765
$\varepsilon_1(0) = \varepsilon_G$	$\varepsilon_b/\varepsilon_r$	0.482
$\hat{\ell}$	Polymer length/ $2/\lambda_D$	6.834
\hat{L}	$240 \text{ \AA}/\lambda_D$	28.219
$r_{c1} (\text{\AA})$	[18]	1.62
\hat{u}_{c1}	Based on r_{c1}	2.128
$r_{c2} (\text{\AA})$	[18]	1.95
\hat{u}_{c2}	Based on r_{c2}	1.768
$r_a (\text{\AA})$	Sec. IV C	0.226
\hat{u}_a	Based on used r_a	15.251
C_0	Salt concentration	0.265
\tilde{K}_1	Table IV	1.362×10^{-2}
\tilde{c}_1	Na concentration/ C_0	0.923
\tilde{c}_1	$\tilde{c} \exp(\hat{u}_c/\varepsilon_S)$	14.890
\tilde{K}_2	Table IV	8.571×10^{-4}
\tilde{c}_2	K concentration/ C_0	0.077
\tilde{c}_2	$\tilde{c} \exp(\hat{u}_c/\varepsilon_S)$	0.775
\bar{a}	$\bar{c} \exp[(\hat{u}_a - \hat{u}_c)/\varepsilon_S]$	4.536×10^8
g_0	GAG concentration/ C_0	10.774
$\hat{\sigma}_1$		0
$\hat{\sigma}_2$		0
T (K)		310.15
α	Used value	0.1

was expected since the dissociation constant for potassium is much smaller than the dissociation constant for sodium and the outward Born force is lower for potassium. On the salt side, it is seen that sodium is the dominant cation with 12 times the concentration of potassium. The potential shows the same overshoot seen in Figs. 3 and 5 due to sodium. Similarly, the force density traverses the brush edge right-left-right-left as seen in Fig. 7(a).

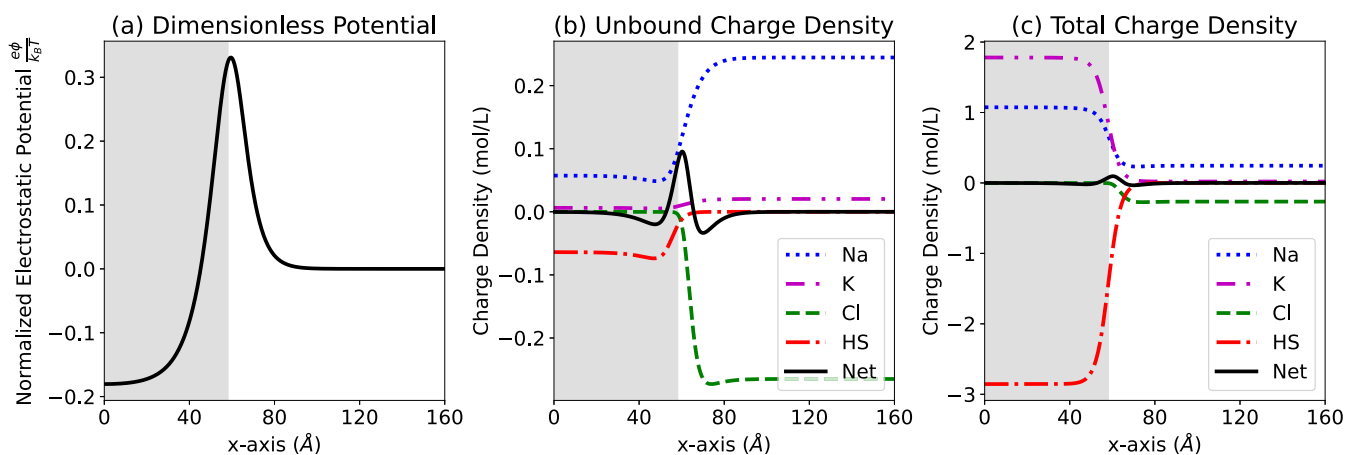


FIG. 8. Two cation sample results. (a) Dimensionless potential, (b) Unbound charge density (M), and (c) Total charge density (M) using parameters from Table VII. In (b) and (c) the dashed blue curve represents Na, the dashed dot dot magenta curve represents K, the dotted green curve represents Cl, the dashed dot red curve represents Heparin, and the solid black curve represents the net charge density. All curves continue flat from 160 to 240 Å. Shaded region represents the GAG region.

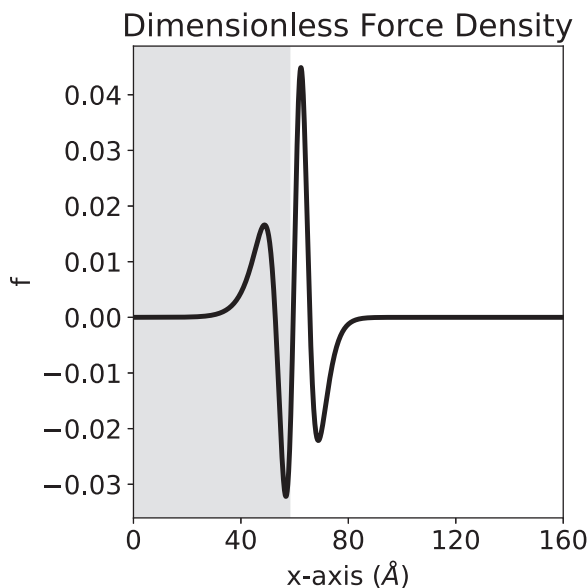


FIG. 9. Dimensionless force density for two cations.

VI. CONCLUSION

We have developed steady-state equilibrium mean-field models for GAG brushes that capture ion partitioning, ion pairing, and varying permittivity effects in GAG brushes. Our models build upon previous Poisson-Boltzmann models [13,19] and generate the same predicted performance when applying our model in the appropriate limits. We have also shown that our model predictions agree well with the molecular simulation data [14], however our model requires the anion

Born radius to be much smaller than typical values found in the literature [18]. The requirement that this unrealistic, non-physical ion hydration radius be used to match experimental or molecular dynamics simulation data appears to be a known challenge for Poisson-Boltzmann based models [20]. Furthermore, there is evidence from neutron diffraction experiments on concentrated salt solutions that the chloride ion disrupts the hydrogen-bond network of bulk water much less than the cations; effects that are not captured using the Born hydration formulation implemented herein [21]. Another explanation is that there are additional energy terms such as GAG dipole effects that our model is neglecting. Further research is needed in this area.

While we have presented a model where the permittivity is a simple function of x , others have proposed a dependence of the permittivity on ion concentrations (*dielectric decrement*) [17,22,23]. Future work will entail exploring the appropriate relationship between permittivity and local environment (including dielectric decrement and biopolymer contributions) and incorporating such a constitutive relationship into our model.

The models presented here offer biophysical detail of biological environments that have anionic beds of macromolecules that attain electroneutrality via atomic cations and cationic residues of proteins. The extent to which such biophysical detail can be used to develop new diagnostics, drug-delivery platforms, or therapeutics remains to be seen.

ACKNOWLEDGMENT

We thank the BLAIS Foundation Fund at CGU for its support of this research.

-
- [1] P. De Gennes, *Adv. Colloid Interface Sci.* **27**, 189 (1987).
 - [2] M. Ballauff and O. Borisov, *Curr. Opin. Colloid Interface Sci.* **11**, 316 (2006).
 - [3] J. Yu, N. E. Jackson, X. Xu, B. K. Brettmann, M. Ruths, J. J. De Pablo, and M. Tirrell, *Sci. Adv.* **3**, eaao1497 (2017).
 - [4] R. Zimmermann, J. F. Duval, C. Werner, and J. D. Sterling, *Curr. Opin. Colloid Interface Sci.* **59**, 101590 (2022).
 - [5] S. F. Shimobayashi, P. Ronceray, D. W. Sanders, M. P. Haataja, and C. P. Brangwynne, *Nature (London)* **599**, 503 (2021).
 - [6] S. Xue, F. Zhou, T. Zhao, H. Zhao, X. Wang, L. Chen, J.-p. Li, and S.-Z. Luo, *Nat. Commun.* **13**, 1112 (2022).
 - [7] E. Astoricchio, C. Alfano, L. Rajendran, P. A. Temussi, and A. Pastore, *Trends Biochem. Sci.* **45**, 706 (2020).
 - [8] C. E. Sing and S. L. Perry, *Soft Matter* **16**, 2885 (2020).
 - [9] J. T. Granados-Riveron and G. Aquino-Jarquín, *Biomed. Pharmacother.* **142**, 111953 (2021).
 - [10] V. P. Narayanaswamy, L. L. Keagy, K. Duris, W. Wiesmann, A. J. Loughran, S. M. Townsend, and S. Baker, *Front. Microbiol.* **9**, 1724 (2018).
 - [11] A. B. Edwards, F. L. Mastaglia, N. W. Knuckey, and B. P. Meloni, *Drug Safety* **43**, 957 (2020).
 - [12] A. Naji, M. Kanduč, J. Forsman, and R. Podgornik, *J. Chem. Phys.* **139**, 150901 (2013).
 - [13] D. Dean, J. Seog, C. Ortiz, and A. J. Grodzinsky, *Langmuir* **19**, 5526 (2003).
 - [14] J. D. Sterling, W. Jiang, W. M. Botello-Smith, and Y. L. Luo, *J. Phys. Chem. B* **125**, 2771 (2021).
 - [15] M. Born, *Z. Phys.* **1**, 45 (1920).
 - [16] Z.-G. Wang, *Phys. Rev. E* **81**, 021501 (2010).
 - [17] J. López-García, J. Horno, and C. Grosse, *Adv. Mater. Sci. Eng.* **2018**, 4316894 (2018).
 - [18] L. Sun, X. Liang, N. v. Solms, and G. M. Kontogeorgis, *Eng. Chem. Res.* **59**, 11790 (2020).
 - [19] J. D. Sterling and S. M. Baker, *Colloid Interface Sci. Commun.* **20**, 9 (2017).
 - [20] B. B. Eakins, S. D. Patel, A. P. Kalra, V. Rezania, K. Shankar, and J. A. Tuszynski, *Front. Mol. Biosci.* **8**, 650757 (2021).
 - [21] R. Mancinelli, A. Botti, F. Bruni, M. Ricci, and A. Soper, *J. Phys. Chem. B* **111**, 13570 (2007).
 - [22] D. Ben-Yaakov, D. Andelman, and R. Podgornik, *J. Chem. Phys.* **134**, 074705 (2011).
 - [23] N. Gavish and K. Promislow, *Phys. Rev. E* **94**, 012611 (2016).